Revealing Controllable Nanowire Transformation through Cationic Exchange for RRAM Application

Chun-Wei Huang, Jui-Yuan Chen, Chung-Hua Chiu, and Wen-Wei Wu*

Department of Materials Science and Engineering, National Chiao Tung University, Hsinchu 300, Taiwan

S *Supporting Information*

ABSTRACT: One dimensional metal oxide nanostructures have attracted much attention owing to their fascinating functional properties. Among them, piezoelectricity and photocatalysts along with their related materials have stirred significant interests and widespread studies in recent years. In this work, we successfully transformed piezoelectric ZnO into photocatalytic TiO_2 and formed TiO_2/ZnO axial heterostructure nanowires with flat interfaces by solid to solid cationic exchange reactions in high vacuum (approximately 10^{-8} Torr) transmission electron microscope (TEM). Kinetic behavior of the single crystalline TiO_2 was systematically analyzed. The nanoscale growth rate of TiO_2 has been measured using in situ TEM videos. On the basis of the rate, we can control the dimensions of the axial-nanoheterostructure. In addition, the unique Pt/ ZnO / TiO_2/ ZnO /Pt heterostructures with complementary resistive switching (CRS) characteristics were designed to solve the important issue of sneak-peak current. The resistive switching behavior was attributed to the migration of oxygen and TiO_2 layer served as reservoir, which was confirmed by energy dispersive spectrometry (EDS) analysis. This study not only supplied a distinct method to explore the transformation mechanisms but also exhibited the potential application of ZnO/TiO_2 heterostructure in nanoscale crossbar array resistive random-access memory (RRAM).

KEYWORDS: *Cationic exchange, RRAM, in situ TEM, ZnO, TiO_2, axial nanowire heterostructures*
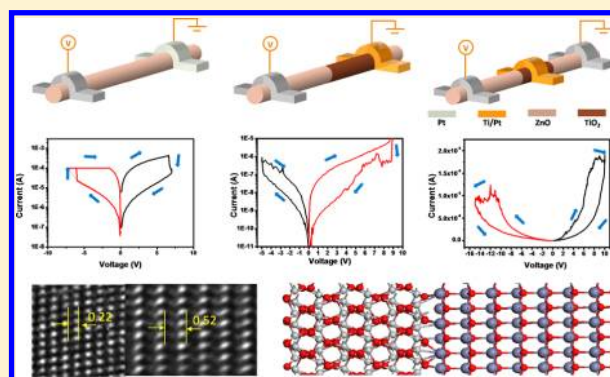
Over the past decades, researchers are increasingly enthralled by one-dimensional metal oxides to develop and expand their functionality. Metal oxides not only inherit the remarkable properties from bulk such as electromechanical and electrochemical properties[1,2] but also exhibit special geometric/anisotropic property and size effect in the research of photodetectors,[3] single-electron transistors,[4] electron emitters,[5] light-emitting diodes,[6] biology,[7] and ultraviolet nanolasers.[8] Among various metal oxides, ZnO and TiO_2 are the most important materials for their potential applications in piezoelectronics, energy harvesting,[9] photocatalysts,[10,11] and resistive switching random access memory.[12–14] Owing to the perfectly aligned band diagram of TiO_2 and ZnO, the electron and hole transfer easily between their conduction and valence bands. As a result, the separation of photogenerated charge carriers is easier compared with a single metal oxide.[15] Recently, extensive investigations have been concentrated on the design and synthesis of crystalline ZnO/TiO_2 heterostructures and/or a compound to improve the quantum efficiency of photocatalysts for applications in water purification.[15] Previous reports have focused on the provision of ZnO/TiO_2 systems by various techniques, including magnetron sputtering,[16] sol−gel,[17] thermal treatment of powers,[18] and liquid phase routes.[19,20] In most cases, solid to solid reactions will lead to the formation of ternary Zn/Ti/O species.[21–23] Two of the most significant mechanisms of solid to solid reactions for nanostructures are

Kirkendall effect[24,25] and ion exchange.[26–28] The Kirkendall effect has been proven to generate hollow nanostructures but is not a common method to create nanomaterials of diverse morphologies. However, ion exchange reaction has been manifested to be an effective method to alter the chemical composition of inorganic nanocrystals by adjusting the reactants. Therefore, ion exchange reaction is advantageous to obtain complex devices for now. Additionally, solid-state ion exchange reaction is still not fully understood. For this purpose, the observation of cationic exchange is also essential for the study of the reaction process.

In situ transmission electron microscope (TEM) is a powerful tool[13,14,29–36] for the study of growth kinetics. In this work, we designed a fascinating method to transform ZnO into TiO_2 through solid to solid cationic exchange reaction in high vacuum in situ TEM. Our method allowed us to study the growth process and reaction mechanism of ionic exchange and oxide material transformation at high temperature. In addition, the ZnO/TiO_2 axial nanoheterostructure had been demonstrated and processed into the device, which exhibited remarkable resistive random-access memory (RRAM) properties. Our experiment results provide the critical insights and

knowledge into the metal oxide transformation and illustrate practical examples of axial heterostructures in crossbar random-access memory.

Single crystalline ZnO nanowires with high aspect ratio were synthesized on Si (100) substrates in a three-zone furnace using the carbothermal reduction method through a vapor–liquid–solid mechanism. Mixed powders of zinc oxide and carbon with a mass ratio of 2:1 were placed upstream of the gas flow and the Au-coated (100) silicon substrates were placed downstream. The temperatures of upstream and downstream were held at 950 and 750 °C, respectively. The temperatures elevated at the rate of 10 °C per min and were held for 90 min. Argon and oxygen flowed as carrier gases at the rate of 100 and 10 sccm, respectively. After the growth process, the furnace cooled down to room temperature. Figure 1a–e is a schematic illustration of
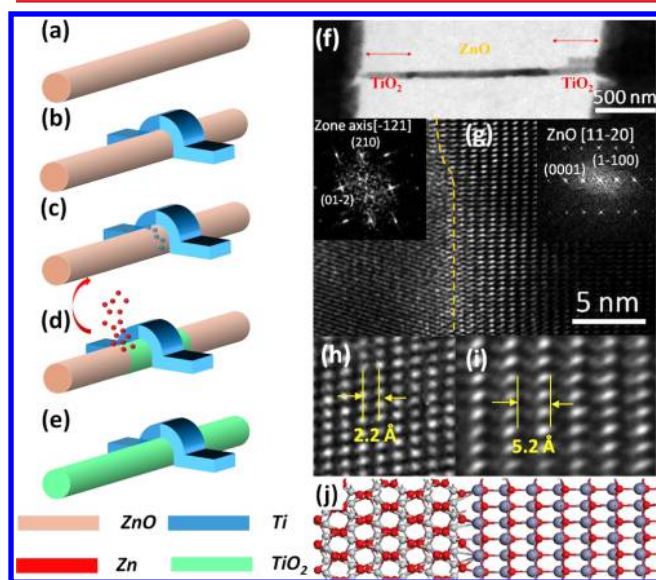
Figure 1. Schematic illustration of the transformation process from ZnO nanowires to ZnO/TiO$_2$ nanowire heterostructures and TEM images of ZnO/TiO$_2$ nanoheterostructures formed through cationic exchange. (a) Single-crystalline ZnO nanowires grown by a vapor–liquid–solid mechanism. (b) ZnO nanowire covered with Ti pad to define the reaction range. (c) Titanium atoms diffused into ZnO lattice at 700 °C, and then the Zn site was replaced with Ti atom. (d) Zn atoms evaporated to vacuum chamber, and ZnO/TiO$_2$ nanoheterostructures and (e) TiO$_2$ were formed. (f) Low magnification TEM image of a ZnO/TiO$_2$ nanoheterostructure by cationic exchange at 700 °C for 3 h. Note that the light contrast is TiO$_2$ and dark contrast is ZnO. (g) A closer view of the TiO$_2$ and ZnO interface, and the insets are the corresponding FFT electron diffraction patterns showing the [$\bar{1}$21] zone axis of TiO$_2$ and [11$\bar{2}$0] of ZnO, respectively. (h,i) High-resolution TEM images of TiO$_2$ and ZnO. (j) The theoretical model of rutile TiO$_2$ (01$\bar{2}$) plane connected with the wurtzite ZnO (0001) plane by Materials Studio software.

the formation process from ZnO to TiO$_2$ nanowire. ZnO nanowires were detached from the wafer into ethanol solution and then dropped on substrates with Si$_3$N$_4$ membrane windows, which was grown by low pressure chemical vapor deposition with thickness of 30 nm (Figure 1a). Methyl methacrylate (bottom layer) and poly(methyl methacrylate) (top layer) were coated as positive tone photoresists (PR), followed by 180 °C baking for 1 min and e-beam lithography. Two hundred nanometers of titanium and 50 nm of platinum were deposited by electron gun deposition system. After

deposition, the PR were removed by lift-off process in acetone (Figure 1b). Direct observation of the cationic exchange reaction via ZnO nanowire and reactive electrodes were carried out in a JEOL 2100F high vacuum TEM. The base pressure in the sample stage was about 3×10^{-8} Torr, and the ion exchange process of the ZnO/TiO$_2$ nanowire heterostructures was performed at the temperature of 700 °C. The replaced Zn atoms evaporated to vacuum chamber after cationic exchange to form TiO$_2$ nanowire, as shown in Figure 1c–e. The in situ TEM was equipped with a video recorder with 1/30 s time resolution. High-resolution lattice imaging and mapping were performed in a Cs-corrected scanning transmission electron microscope (STEM, JEOL ARM 200F) with an energy dispersive spectrometer (EDS). The resistive switching behaviors of the ZnO/TiO$_2$ nanowire were measured by an Agilent 4145B system at room temperature in ambient conditions.

Figure 1 is a schematic illustration of the formation process from ZnO to TiO$_2$ nanowire and heterostructure morphology. The crystalline structure of ZnO/TiO$_2$ nanowire through cationic exchange was revealed. Figure 1a–e shows the details of the formation process from ZnO to TiO$_2$ nanowire. Figure 1f shows the low magnification TEM image of a TiO$_2$/ZnO axial heteronanowire. The sharp interface between wurtzite ZnO and rutile TiO$_2$ in Figure 1g demonstrated the epitaxial relation-ships across the interface, which are ZnO (1$\bar{1}$00)//TiO$_2$ (210) and [11$\bar{2}$0]// [$\bar{1}$21], respectively. Figure 1h,i shows the HRTEM images locally enlarged in Figure 1g, which indicated that TiO$_2$ and ZnO nanowires were single-crystalline. The structure of cationic-exchanged TiO$_2$ nanowire has been identified from both the fast Fourier transform diffraction pattern (FFTDP) and HRTEM, demonstrating TiO$_2$ is of rutile structure and tetragonal system (space group $P4_2/mnm$). Moreover, the theoretical model of rutile TiO$_2$ (01$\bar{2}$) connecting with the wurtzite ZnO (0001) was simulated by Materials Studio software, as shown in Figure 1j.

The high-angle annular dark-field imaging (HAADF) and EDS mapping of as-reacted nanowire (ZnO) and cationic-exchanged heteronanowire (ZnO/TiO$_2$) are shown in Figure 2. The HAADF STEM image of the initial ZnO nanowire with patterned Ti/Pt pad is shown in Figure 2a. Figure 2b–d gives the EDS mapping, showing the element distribution of Zn, O, and Ti. The signal in EDS mapping of Ti layer and ZnO nanowire interface are clean without overlapping. The cationic exchanged HADDF image is shown in Figure 2f. The dark contrast in HAADF image indicated the richness of titanium due to its light atomic weight. Figure 2g–i shows the elemental distribution in the axial heteronanowire. The oxygen ion remained but zinc was partially replaced by titanium after the solid to solid cationic exchange process. Figure 2e,j gives the schematic illustrations of the ZnO nanowire and TiO$_2$/ZnO axial heteronanowire.

To further understand the formation behavior, in situ observation of the solid to solid cationic exchange process is essential. Figure 3a–d gives the in situ TEM images recorded from an in situ video. In each figure, the red arrow points out the reaction interface. The recorded images are critical evidence of the reaction progression (please refer to Supporting Information Video 1). During the cationic exchange process at high temperature, ZnO nanowire is not thermally stable and Ti element preferred to form crystalline TiO$_2$ structure. Therefore, Ti atoms would diffuse into ZnO nanowire and replaced Zn atoms. Then, Ti combined with oxygen to form
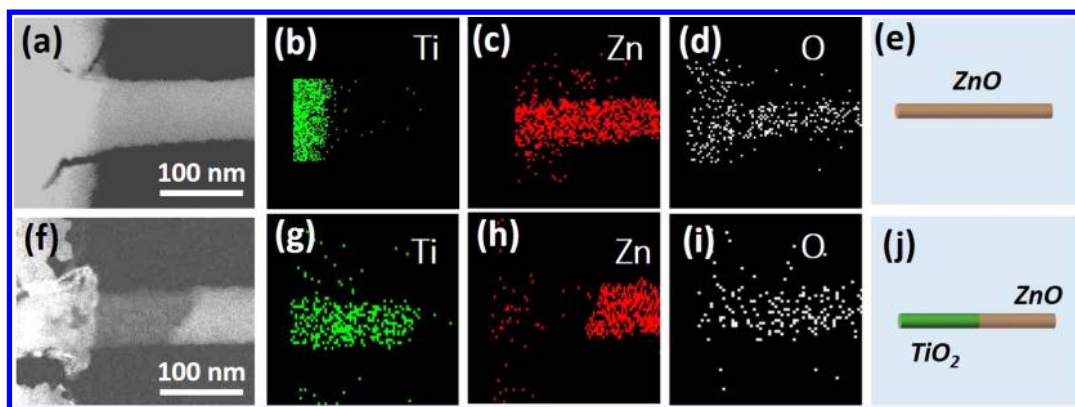
Figure 2. HAADF STEM images and EDS mapping of as-reacted nanowire (ZnO) and cationic-exchanged heteronanowire (ZnO/TiO$_2$). (a) HAADF STEM image shows initial ZnO nanowire and Ti metal pad. (b−d) EDS mapping shows the Zn, O, and Ti distribution. The Ti layer and ZnO nanowire interface are sharp and clean. (f) HADDF STEM image shows the TiO$_2$ and ZnO interface. (g−i) EDS mapping shows the Ti element diffused into ZnO nanowire and replaced Zn to form TiO$_2$. (e,j) Schematic illustration of the ZnO nanowire and TiO$_2$/ZnO nanoheterostructures.
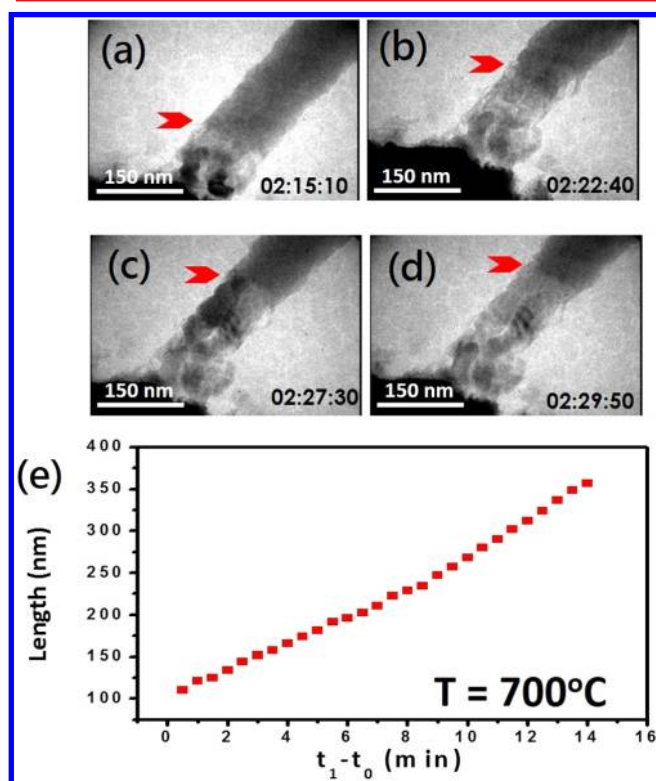
Figure 3. Series of images clipped from the video showing the formation process by solid to solid cationic exchange at 700 °C. The numbers in lower right corner follow hours, minutes, and seconds. The red arrow highlights the position of the interface. The images were obtained at elapsed times: (a) 02:15:10, (b) 02:22:40, (c) 02:27:30, and (d) 02:29:50. (e) Plot of growth length of TiO$_2$ as a function of time.

TiO$_2$ at 700 °C in a high vacuum TEM chamber. The EDS line scan of the ZnO/TiO$_2$ interface can be seen in Supporting Information Figure S1. The replaced zinc was evaporated to a vacuum chamber after being cationically exchanged. The formation reaction can be described as follows:

$$2ZnO_{(S)} + Ti_{(S)} = TiO_{2(S)} + 2Zn_{(V)}$$
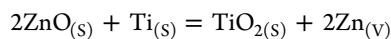
Different electronegativity and high vacuum are essential for inducing cationic exchange behavior in metal oxide systems.

Different electronegativity results in substitution of metal elements. The electronegativities of zinc and titanium elements are 1.65 and 1.54, respectively, indicating that the electron is prone to be captured by zinc atom. Inversely, titanium has a higher tendency toward bonding with oxygen than zinc. However, in high vacuum systems, the rare oxygen atmosphere prevented nanowires from forming ternary compounds. In this work, titanium exhibits stronger oxidation activity and capacity than zinc. Additionally, the high vacuum TEM chamber lead to dilute oxygen concentration. As a result, Ti atoms tend to grab the oxygen from ZnO and then form TiO$_2$ (Supporting Information Figure S2). For comparison, we have designed an experiment to anneal ZnO nanowire with Ti pads under the same condition but in ambient atmosphere. A new crystalline structure, twin-involved Zn$_2$TiO$_4$ phase, was observed and shown in Supporting Information Figure S3. The spinel Zn$_2$TiO$_4$ nanowire with twin structure was reported by Yang et al.[22] and resulted from reducing the free energy. The element distribution in the multi-twinned spinel nanowire was displayed in Supporting Information Figure S4. A schematic diagram shows a different formation mechanism under two extreme annealing atmospheres (Supporting Information Figure S5). Figure 3e shows a plot of growth length of TiO$_2$ as a function of time. On the basis of the statistics, the average reaction rate along the axial direction is about 18 nm min^{-1}. The TiO$_2$ growth rate is linear, and there is no stagnation on the plot. Thus, the main mechanism is the interfacial reaction control in solid to solid reaction.

The transformation of ZnO into other metal oxides is a special behavior through solid to solid reaction. In previous studies, ZnO nanowire reacted with metal elements to form Z$_x$/C$_y$/O$_z$ (C = Ti, Mg, Al, etc.) ternary species.[22,23,25] However, we obtained binary and single crystalline TiO$_2$ by cationic exchange. It is worth mentioning that we can modulate the reactants to fabricate various heterojuctions by electronegativity differences in high vacuum systems. Those heterojuctions can expand the application in different fields and benefit us to understand the interface effect by designing materials for applications in electronic, photonic, magnetic, and thermal characteristics. In our work, the as-formed ZnO/TiO$_2$ heterojunction was made into nonvolatile resistive memory to study small size effects.
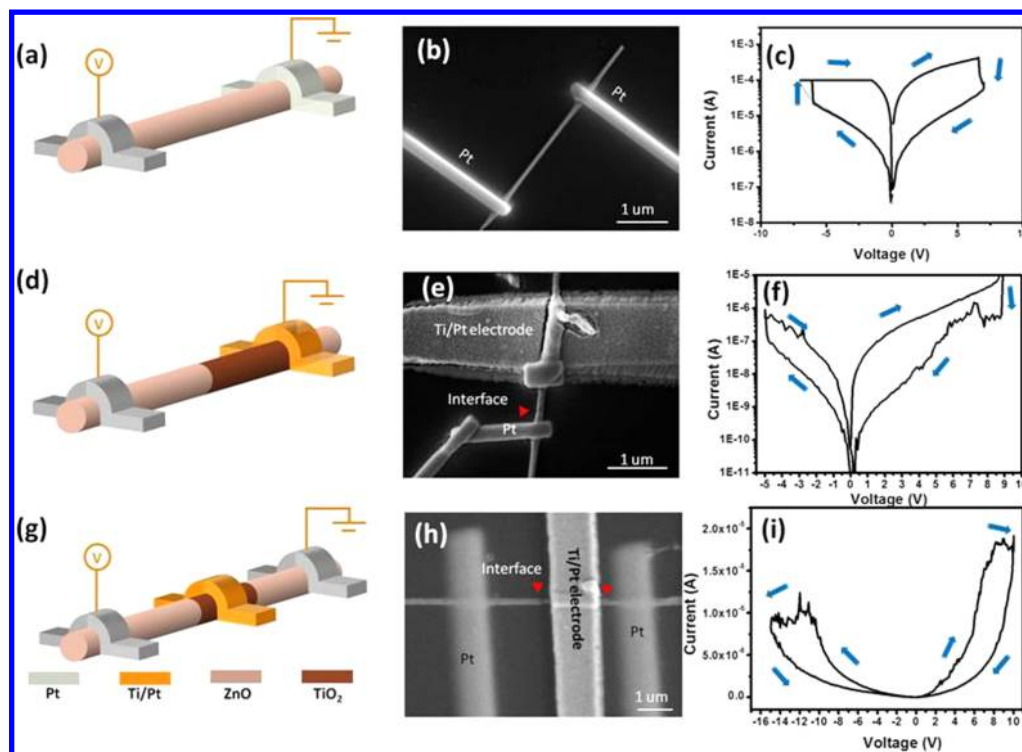
Figure 4. Different bipolar RRAM devices and their switching behavior in ZnO, ZnO/TiO$_2$, and ZnO/TiO$_2$/ZnO. (a,d,g) Schematic diagram of ZnO nanowire, bilayer (ZnO/TiO$_2$), and trilayer nanowire (ZnO/TiO$_2$/ZnO) with grounded right-hand-side. (b,e,h) Corresponding SEM images of three types of nanowires with Pt electrodes. (c) Typical bipolar resistive switching behavior. (f) The switching loop is clockwise in both positive and negative bias. (i) The switching loop is clockwise in negative bias and counterclockwise in positive bias.

ZnO with RRAM properties has been reported in many studies.[13,14,37−40] In addition, the scaling down of RRAM devices is strongly desired not only for understanding the switching mechanisms at sublithographic scale but also for improving the characteristics. In this work, we compared three types of components, revealing the potential of heterostructure in high density memory array. Figure 4 shows different bipolar RRAM devices and its switching behavior in ZnO, ZnO/TiO$_2$, and ZnO/TiO$_2$/ZnO nanowire. We applied bias to left-hand side and grounded the right-hand side, as shown in Figure 4a,d,g. First, the simple ZnO device was measured as the reference with the following devices. Figure 4a is a schematic diagram of ZnO nanowire with typically bipolar resistive switching behavior, as shown in Figure 4c. The corresponding SEM image is shown in Figure 4b. The SET voltage was −6.25 V with 10^{-4} A current compliance; whereas the RESET voltage was 7 V. Next, the bilayer of ZnO/TiO$_2$ was measured. Figure 4d is a schematic diagram of bilayered resistive switching device with ZnO/TiO$_2$ interface, which is known as MISM (metal–isolator–semiconductor–metal) structure. The red arrow marked in Figure 4e is the interface of ZnO and TiO$_2$. The SET/RESET voltage is −5 V/9 V, respectively. Typical switching behavior is shown in Figure 4f, and the switching loop is clockwise in both positive and negative bias. The resistive switching can be attributed to the oxygen vacancy exchange between the ZnO and TiO$_2$ layers. The TEM−EDS data are included in Supporting Information Figure S6. The advantage of ZnO/TiO$_2$ bilayer is that TiO$_2$ serves as an oxygen reservoir. Besides, TiO$_2$ layer can prevent overload current as the device switches to the ON state, resulting in gradually rising/dropping at SET/RESET voltage and strengthening the reliability of the device. Finally, the

complementary resistive switching (CRS) device was designed to solve the important issue of sneak-peak current because it would be written into the OFF state after the reading process.[41,42] Figure 4g is a schematic diagram of CRS device in trilayer memristor. Detailed fabrication process can be referred to Supporting Information Figure S7. The both ends of ZnO can be regarded as memristor 1 and memristor 2. The equivalent circuit of the trilayer memristor is an antiseries of two memristors. The I−V characteristics of the CRS device is shown in Figure 4i. Unlike the MISM system, the switching loop is clockwise in negative bias and counterclockwise in positive bias. When the voltage was raised to −9 V, memristor 1 switched to the ON state. The current gradually decreased as the bias increased from −12 to −18 V since memristor 2 would switch to the OFF state. Similarly, memristor 2 switched to the ON state at about 7 V, and memristor 1 switched to the OFF state at 10 V. The switching state from negative to positive bias is 10 → 11 → 01 → 11 → 10 ('1' is the ON state and 0 is the OFF state, and the first number is the state for memristor 1 and the second number is for memristor 2). The nonreading device will remain in a high resistance state, which can avoid interfering with the measuring device. The nonoverlap of the I−V curve in small bias may be caused by different resistances of memristor 1 and 2, as shown in Figure 4h. Obviously, a difference in length of ZnO resulted in the divergence of the 10 and 01 states. In short, the CRS device exhibits high resistance independent of the stored information and makes the application of high density memory array architectures feasible. Multiple cycles measurement of the CRS device were included in the Supporting Information Figure S8.

In summary, the feasibility to transform ZnO to TiO$_2$ nanowire through solid to solid cationic exchange reaction

has been identified. The structure and chemical composition were investigated by TEM and EDS. In the in situ observation of the solid to solid reaction, Ti element formed TiO_2 in high vacuum TEM. We observed the ZnO/TiO_2 transformation in real time, providing that the evolution mechanism was interfacial control. The average reaction rate along the axial direction is about 18 nm min^{-1}. The CRS device in trilayer $ZnO/TiO_2/ZnO$ nanowire demonstrated the feasibility to apply these in high density memory array architectures. The resistive switching can be attributed to the oxygen exchange between the ZnO and TiO_2. In this investigation, a useful cationic exchange method has been developed to transform ZnO into TiO_2 nanowire, which can acquire the ZnO/TiO_2 nanoheterostructures for extensive applications.

■ ASSOCIATED CONTENT

Ⓢ Supporting Information

Proof that ZnO transforms to TiO_2 nanowire through solid to solid cationic exchange reaction and an in situ TEM video to provide the evidence of direct observation of the formation process. This material is available free of charge via the Internet at http://pubs.acs.org.

■ AUTHOR INFORMATION

Corresponding Author

*(W.-W.W.) E-mail: wwwu@mail.nctu.edu.tw.

Author Contributions

C.-W.H. fabricated the sample and the in situ reaction experiments. C.-W.H. and J.-Y.C. performed electrical switching experiments. C.-W.H. and C.H.C. performed the in situ reaction experiments. C.-W.H. and W.-W.W. analyzed the diffraction data and atomic structure. C.-W.H. and W.-W.W. conceived the study and designed the research. C.-W.H. performed the experiments with the support from W.-W.W. and W.-W.W. wrote the paper.

Notes

The authors declare no competing financial interest.

■ ACKNOWLEDGMENTS

■ REFERENCES

(1) Pan, Z. W.; Dai, Z. R.; Wang, Z. L. *Science* **2001**, *291*, 1947.

(2) Hu, J. T.; Odom, T. W.; Lieber, C. M. *Acc. Chem. Res.* **1999**, *32*, 435.

(3) Zhai, T.; Fang, X.; Liao, M.; Xu, X.; Zeng, H.; Yoshio, B.; Golberg, D. *Sensors* **2009**, *9*, 6504.

(4) Cheng, G.; Siles, P. F.; Bi, F.; Cen, C.; Bogorin, D. F.; Bark, C. W.; Folkman, C. M.; Park, J.-W.; Eom, C.-B.; Medeiros-Ribeiro, G.; Levy, J. *Nat. Nanotechnol.* **2011**, *6*, 343.

(5) Lee, C. J.; Lee, T. J.; Lyu, S. C.; Zhang, Y.; Ruh, H.; Lee, H. J. *Appl. Phys. Lett.* **2002**, *81*, 3648.

(6) Caruge, J. M.; Halpert, J. E.; Wood, V.; Bulovic, V.; Bawendi, M. G. *Nat. Photonics* **2008**, *2*, 247.

(7) Knez, M.; Kadri, A.; Wege, C.; Gösele, U.; Jeske, H.; Nielsch, K. *Nano Lett.* **2006**, *6*, 1172.

(8) Huang, M. H.; Mao, S.; Feick, H.; Yan, H.; Wu, Y.; Kind, H.; Weber, E.; Russo, R.; Yang, P. *Science* **2001**, *292*, 1897.

(9) Wang, Z. L.; Song, J. H. *Science* **2006**, *312*, 242.

(10) Linsebigler, A. L.; Lu, G. Q.; Yates, J. T. *Chem. Rev.* **1995**, *95*, 735.

(11) Hashimoto, K.; Irie, H.; Fujishima, A. *Jpn. J. Appl. Phys.* **2005**, *44*, 8269.

(12) Kwon, D. H.; Kim, K. M.; Jang, J. H.; Jeon, J. M.; Lee, M. H.; Kim, G. H.; Li, X. S.; Park, G. S.; Lee, B.; Han, S.; Kim, M.; Hwang, C. S. *Nat. Nanotechnol.* **2010**, *5*, 148.

(13) Chen, J. Y.; Hsin, C. L.; Huang, C. W.; Chiu, C. H.; Huang, Y. T.; Lin, S. J.; Wu, W. W.; Chen, L. J. *Nano Lett.* **2013**, *13*, 3671.

(14) Huang, Y. T.; Yu, S. Y.; Hsin, C. L.; Huang, C. W.; Kang, C. F.; Chu, F. H.; Chen, J. Y.; Hu, J. C.; Chen, L. T.; He, J. H.; Wu, W. W. *Anal. Chem.* **2013**, *85*, 3955.

(15) Chong, M. N.; Jin, B.; Chow, C. W. K.; Saint, C. *Water Res.* **2010**, *44*, 2997.

(16) Cheng, C.; Li, W.; Wong, T. L.; Ho, K. M.; Fung, K. K.; Wang, N. *J. Phys. Chem. C* **2011**, *115*, 78.

(17) Wu, W.; Cai, Y. W.; Chen, J. F.; Shen, S. L.; Martin, A.; Wen, L. X. *J. Mater. Sci.* **2006**, *41*, 5845.

(18) Zhu, B. L.; Xie, C. S.; Wang, W. Y.; Huang, K. J.; Hu, J. H. *Mater. Lett.* **2004**, *58*, 624.

(19) Yang, H. G.; Zeng, H. C. *J. Am. Chem. Soc.* **2004**, *127*, 270.

(20) Mane, R. S.; Lee, W. J.; Pathan, H. M.; Han, S.-H. *J. Phys. Chem. B* **2005**, *109*, 24254.

(21) Ocana, M.; Hsu, W. P.; Matijevic, E. *Langmuir* **1991**, *7*, 2911.

(22) Yang, Y.; Scholz, R.; Fan, H. J.; Hesse, D.; Gosele, U.; Zacharias, M. *ACS Nano* **2009**, *3*, 555.

(23) Yang, Y.; Sun, X. W.; Tay, B. K.; Wang, J. X.; Dong, Z. L.; Fan, H. M. *Adv. Mater.* **2007**, *19*, 1839.

(24) Yin, Y. D.; Rioux, R. M.; Erdonmez, C. K.; Hughes, S.; Somorjai, G. A.; Alivisatos, A. P. *Science* **2004**, *304*, 711.

(25) Fan, H. J.; Knez, M.; Scholz, R.; Nielsch, K.; Pippel, E.; Hesse, D.; Zacharias, M.; Gosele, U. *Nat. Mater.* **2006**, *5*, 627.

(26) Son, D. H.; Hughes, S. M.; Yin, Y. D.; Alivisatos, A. P. *Science* **2004**, *306*, 1009.

(27) Robinson, R. D.; Sadtler, B.; Demchenko, D. O.; Erdonmez, C. K.; Wang, L. W.; Alivisatos, A. P. *Science* **2007**, *317*, 355.

(28) Zhang, B.; Jung, Y.; Chung, H. S.; Van Vugt, L.; Agarwal, R. *Nano Lett.* **2010**, *10*, 149.

(29) Hsin, C. L.; Lee, W. F.; Huang, C. T.; Huang, C. W.; Wu, W. W.; Chen, L. J. *Nano Lett.* **2011**, *11*, 4348.

(30) Lu, K. C.; Wu, W. W.; Ouyang, H.; Lin, Y. C.; Huang, Y.; Wang, C. W.; Wu, Z. W.; Huang, C. W.; Chen, L. J.; Tu, K. N. *Nano Lett.* **2011**, *11*, 2753.

(31) Wu, W. W.; Lu, K. C.; Wang, C. W.; Hsieh, H. Y.; Chen, S. Y.; Chou, Y. C.; Yu, S. Y.; Chen, L. J.; Tu, K. N. *Nano Lett.* **2010**, *10*, 3984.

(32) Chen, L. J.; Wu, W. W. *Mater. Sci. Eng., R* **2010**, *70*, 303.

(33) Chen, Y.; Lin, Y. C.; Huang, C. W.; Wang, C. W.; Chen, L. J.; Wu, W. W.; Huang, Y. *Nano Lett.* **2012**, *12*, 3115.

(34) Huang, C. W.; Hsin, C. L.; Wang, C. W.; Chu, F. H.; Kao, C. Y.; Chen, J. Y.; Huang, Y. T.; Lu, K. C.; Wu, W. W.; Chen, L. J. *Nanoscale* **2012**, *4*, 4702.

(35) Chiu, C. H.; Huang, C. W.; Chen, J. Y.; Huang, Y. T.; Hu, J. C.; Chen, L. T.; Hsin, C. L.; Wu, W. W. *Nanoscale* **2013**, *5*, 5086.

(36) Chen, K. C.; Wu, W. W.; Liao, C. N.; Chen, L. J.; Tu, K. N. *Science* **2008**, *321*, 1066.

(37) Yen, D. C.; Chang, W. Y.; Ching, Y. H.; Cheng, Y. C.; Chih, H. H.; Lin, S. J.; Wu, T. B.; Hau, H. *IEEE Trans. Electron Devices* **2011**, *58*, 1735.

(38) Yang, Y.; Zhang, X.; Gao, M.; Zeng, F.; Zhou, W.; Xie, S.; Pan, F. *Nanoscale* **2011**, *3*, 1917.

(39) Qi, J.; Huang, J.; Paul, D.; Ren, J.; Chu, S.; Liu, J. *Nanoscale* **2013**, *5*, 2651.

(40) Chiang, Y. D.; Chang, W. Y.; Ho, C. Y.; Chen, C. Y.; Ho, C. H.; Lin, S. J.; Wu, T. B.; He, J. H. *IEEE Trans. Electron Devices* **2011**, *58*, 1740.

(41) Linn, E.; Rosezin, R.; Kugeler, C.; Waser, R. *Nat. Mater.* **2010**, *9*, 403.

(42) Bae, Y. C.; Lee, A. R.; Lee, J. B.; Koo, J. H.; Kwon, K. C.; Park, J. G.; Im, H. S.; Hong, J. P. *Adv. Funct. Mater.* **2012**, *22*, 709.